1997 HST Calibration Workshop
Space Telescope Science Institute, 1997
S. Casertano, et al., eds.

FGS1R: Potentially HST's Astrometry Science Workhorse

Olivia Lupie, Ed Nelan and Lauretta Nagel

Space Telescope Science Institute, 3700 San Martin Drive Baltimore, MD 21218

Abstract. We review the enhancements to the flight spare FGS (called FGS1R) which was installed in the Second Servicing Mission in February 1997, and present the latest results of the FGS1R monitoring program. The performance of FGS1R and the current astrometer, FGS3, are compared and we present simulations of expected performance of FGS1R once the instrument reaches in-orbit stability.

1. Introduction

The Second Servicing Mission to HST in 1997 included the installation of FGS1R, an enhanced flight spare, to replace the original FGS1 whose mechanical bearings were beginning to wear. In this paper, we review the enhancements to FGS1R and present the latest results of the FGS1R monitoring program. The performance of FGS1R and the current astrometer, FGS3, are compared and we present simulations of expected performance of FGS1R once the instrument reaches in-orbit stability.

Over the past 7 years, in-orbit evaluations of the FGSs have shown that proper alignment of the FGSs' complex array of internal optics is absolutely essential to its performance. Comparison of pre-launch performance with initial in-orbit operation shows that alignments are not preserved during the launch stresses and continuously evolve as the instrument outgasses. Hughes Danbury Optical Systems, the manufacturer of the FGS, prepared a refurbished FGS with a commandable articulating adjustment optic that recenters the light beam onto the critical component of the interferometer, the Koesters prism. The replacement FGS in radial bay #1 contains the AMA, an Articulating Mirror Assembly (also referred to as FF3, Folding Flat 3, in other documentation).

A centered beam on the prism results in an FGS with more dynamic range and resolving power than the current FGS3 astrometer. Simulations indicate that FGS1R will be able to *detect* and *resolve* multiple systems with separations of 5 and 10 mas, respectively.

2. Instrument Overview and the Articulating Folding Flat Mirror

In order to emphasize the benefits of the adjustable transfer mirror, called the Articulating Mirror Assembly (AMA), a brief discussion of the FGSs optical train is in order. Additional detail may be found in Voit (1997).

2.1. The Koesters Prism and FGS Optical Train

The heart of the FGS white-light interferometer consists of a beam splitter followed by two Koesters prisms. The prism is a fused silica pyramid consisting of two halves with a dielectric interface. The beauty of the prism is that it senses the tilt of a wavefront presented to it. As the tilt varies, the signal from the Koesters prism responds in a way that correlates with the angle of tilt. To sense the displacement of the wavefront in two dimensions, each FGS contains two Koesters prisms, oriented orthogonally with respect to one another. The dielectric in the prism divides the beam into two equal parts, with a 90

degree phase difference between the reflected and transmitted portions of the beam, the latter lagging the former. The beam reflected from one side of the prism, when joined with the transmitted beam from the other side, constructively or destructively interferes to a degree depending upon the angle between the incoming wavefront and the entrance face. Each Koesters prism thus emits two collimated exit beams whose relative intensities depend upon the tilt of the incident wavefront. Each beam is focussed and passed through a field stop to illuminate the surface of a photomultiplier tube (PMT), which records the number of photons. A schematic diagram of the Koesters prism is shown in Figure 1.

The entire annulus of the FGS is sampled by the combined motion of the Star Selector Assemblies, A and B (abbreviated SSA and SSB). The SSA, a rigid assembly of mirrors and a five element corrector group, and SSB consisting of four mirrors, can be commanded to rotate about the HST optical axis and transfer the beam to the beam splitter and Koesters prisms. Due to the presence of spherical aberation from the telescope's primary mirror, the modulation and morphology of the S-Curve depends critically upon the precision of the optical alignment of the Koesters prism with respect to the wavefront's axis of tilt. FGS1R has been upgraded from the orginal design by a substitution of an articulating flat mirror mirror for a previously static mirror. This movable mirror can be commanded to align the wavefront on the face of the Koesters prism and thereby restore the S-Curve to the optimal modulation.

3. The S-Curve

The relative intensities of the beam emerging from the Koester's prism correlates with the wavefront tilt, which is in fact controlled by the SSA and SSB rotation. We refer the reader to Voit (1997) for greater detail. The normalized difference of the PMTs versus the position of the IFOV in arcsec produces an *S-Curve*. The S-Curve is the interferometric transfer function. Its morphology and modulation are a direct diagnostic of the performance of the FGS. The X-axis S-curve at each X position is given by the following with a similar expression for Y:

$$S_x = (A_x - B_x)/(A_x + B_x)$$

where A_x and B_x are the PMT counts from PMTs A and B on the X channel. When the IFOV is more than 100 mas from the location of the interferometric null, the PMTs record nearly equal intensities. The zero point crossing between the peaks of the S-Curve occurs near interferometric null in the ideal case (slight differences in the PMT sensitivites and in the optical paths shift the zero-point crossing from the null and have to be adjusted in data reduction). Figure 2 displays a series of FGS1R S-Curves. The solid line is the S-Curve obtained when the FGS1R was accurately aligned. The theoretical modulation amplitude is 1.4 peak-to-peak. Thus the solid-line S-Curve in Figure 2 demonstrates that the performance is very close to specification.

4. Alignment Issues

Figure 1 illustrates a perfect alignment of the Koesters prism with respect to the HST optical axis, i.e., the wavefront's tilt axis is in the plane of the prism's dielectric surface. The S-Curve will be degraded if the tilt axis of the collimated beam from the beamsplitter does not fall on the center of the Koesters prism face. The amount of offset from optimal alignment is termed "decenter". A decentered beam would be illustrated as a shift of position "B" (in that figure) with respect to the center of the face of the prism and the dielectric. The AMA can be adjusted to re-position that beam.

Another adverse effect can occur when the alignment of the optics in the star selectors is not perfect. HDOS believes that a misalignment of the SSB reflective optics and the

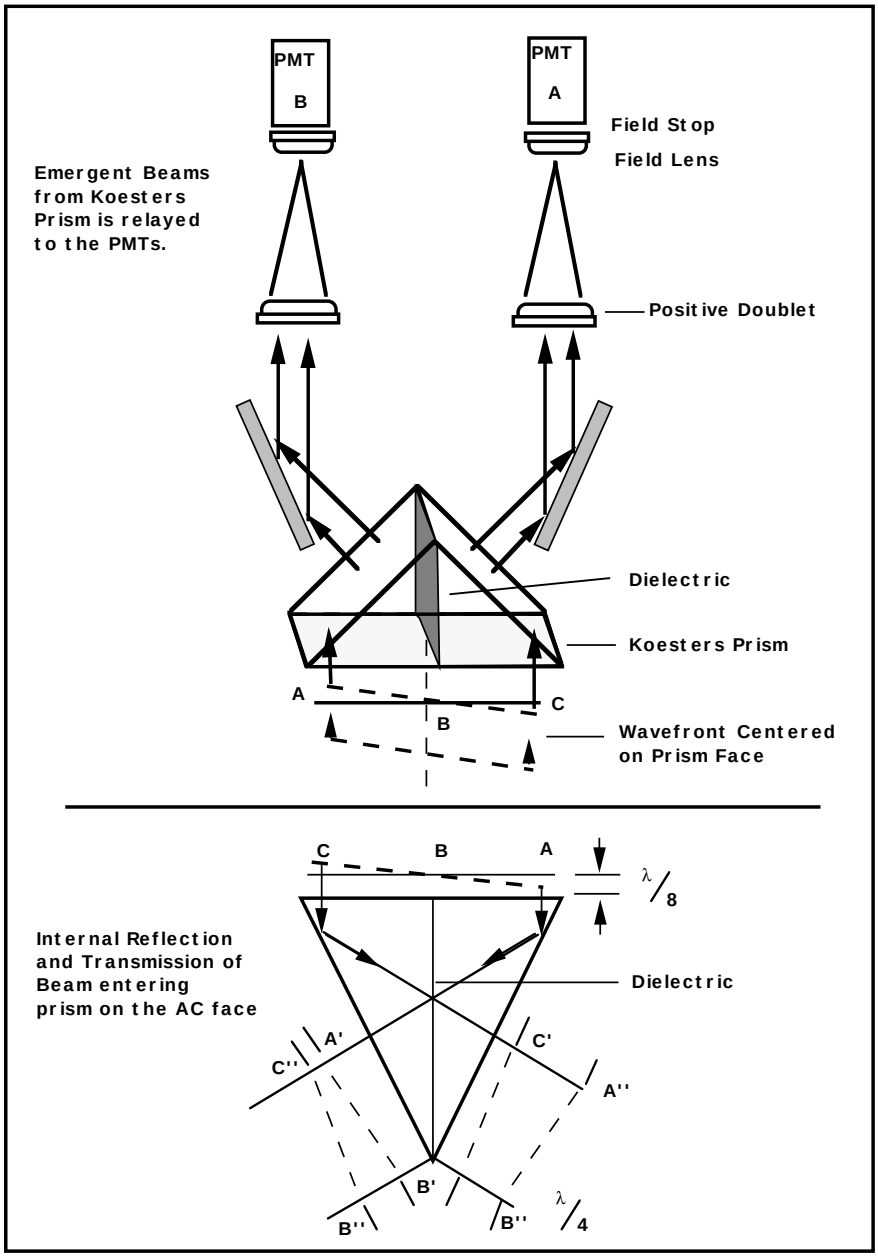

Figure 1. Emergent Beams from the Koesters Prisms are relayed to the PMTs. The Koester prism is sensitive to tilt of the wavefront about an axis which is normal to the page at point B. If the axis of tilt is not at point B, the beam is said to be "decentered."

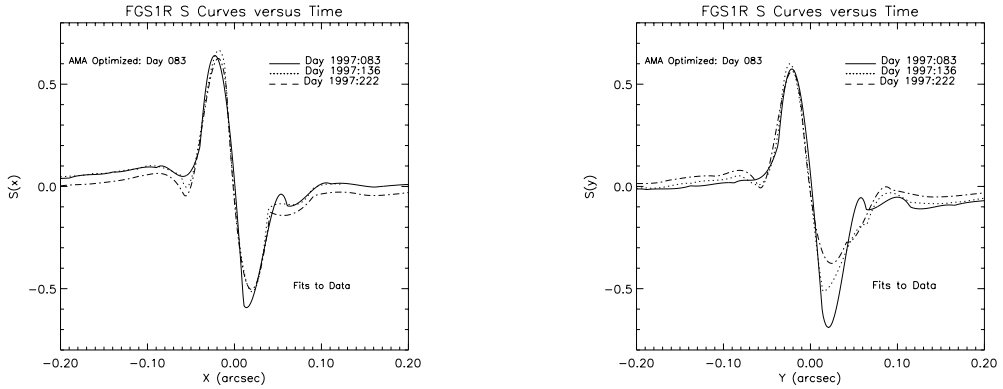

Figure 2. The temporal evolution due to desorption of the FGS1R S curves during Science Mission Orbital Verification. The AMA was re-positioned on day 083.

Koesters prism causes a decentering of the wavefront as the Star Selectors are rotated. The effect gives rise to S-Curve characteristics which vary as a function of location in the annulus. The AMA can optimize the S-Curve at any one place but does not eliminate the field dependence.

The spherical aberration from the HST's misfigured primary mirror presents to the Koesters prism a wavefront with curvature. Consequently, any misalignment in the FGS which results in a decenter of the beam at the Koesters prism will spawn optical aberrations that degrade the S-Curve morphology and modulation. In Figure 2, the Y-axis S-Curve from 1997 day 222 demonstrates this sensitivity. Here, the Koesters prism is decentered by about 0.25 mm and the S-Curve has lost ∼25% of its peak-to-peak amplitude relative to the optimal observation from day 083.

5. The In-Orbit History of FGS1R to Date

The alignment of the FGS1R was measured in-orbit a few weeks after the Servicing Mission and the data revealed that zero gravity effects had altered a near-perfect ground alignment. Several stages in the AMA optimization process were implemented during the Servicing Mission Observatory Verification by the HDOS team with support from GSFC and STScI. A single star (verified by an earlier HST test) and later, the standard (single) star Upgren69 were observed at various places within the annulus and at varying intervals during the verification period. Final optimization of the mirror on day 83 yielded the near-perfect S-Curves in the center of the annulus.

The internal alignment changes as the instrument slowly outgasses. The X and Y S-curves in Figure 2, obtained on three dates (day 083 when the AMA alignment was optimized, and days 136 and 222), clearly reveal an evolving morphology.

The change in modulation amplitude (peak-to-peak) as a function of 1997 day number is plotted in the upper panel of Figure 3 (these data are courtesy of L. Abramowicz-Reed and K. Chisolm, HDOS). HDOS used these data and the morphology signatures to model the corresponding decenter of the beam on the Koesters prism. These results are plotted in the lower panel of Figure 3. A direct correlation between the S-Curve shape (and hence the FGS1R overall performance) and the centering of that beam is clear in these plots. The most recent results of the cycle 7 FGS1R monitoring programs reveal that the FGS1R is still outgassing and its environment is not yet stable but the changes appear to be slowing down with time. In fact, the most recent monitoring data obtained during this '97 Calibration

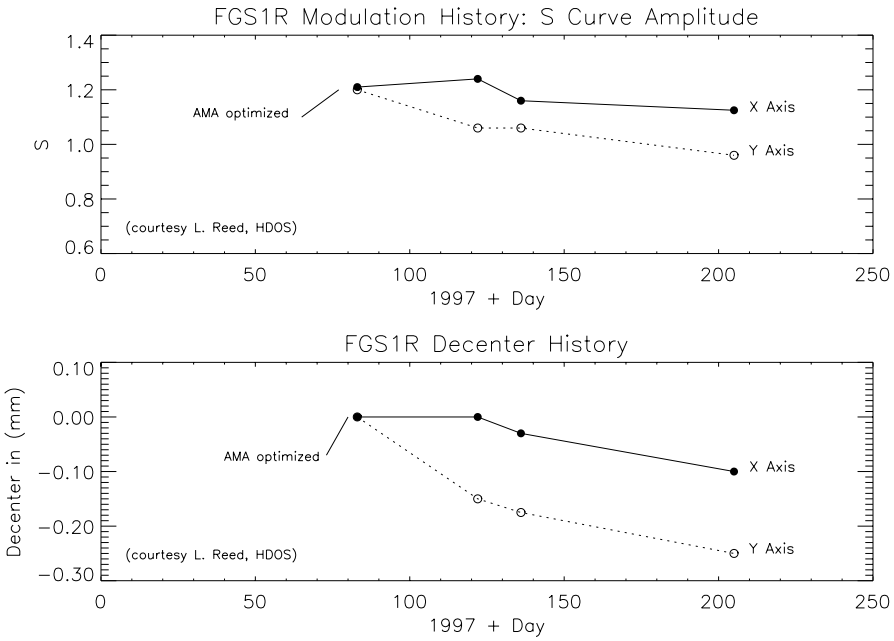

Figure 3. The upper panel contains measurements of the peak-to-peak amplitude of the S-Curves at the center of the annulus (filter F583W) as a function of day number. The lower panel is the corresponding decenter of the beam on the face of the Koesters prism, modelled by HDOS. The data was provided by Abramowicz-Reed and Chisolm, HDOS.

workshop indicate that the stability could occur within the next few months (Abramowicz-Reed 1997). Models of desorption evolution are simple at best because temporal histories of the previous FGSs shortly after orbit insertion are not available.

When the cycle 7 monitoring data indicate FGS1R's stability, the AMA will be adjusted via ground command to optimize the S-Curves. Detailed performance assessment tests and calibrations will ensue.

S-Curve data obtained across the annulus of FGS1R indicate a spatial or field dependence, probably due to small alignment errors in the optical components of the movable star selectors. Although the performance is degraded at the extreme ends of the FGS1R pickle, the overal capabilities of FGS1R exceeds that of the other FGSs.

6. A Brief Review of the FGS1R Cycle 7 Monitoring Program

The cycle 7 calibration plan for FGS1R is primarily a monitoring and assessment program and contains the following tests. If so justified by the results of the cycle 7 program, FGS1R will be calibrated as an astrometric instrument starting in Cycle 8.

1. Proposal 7678, *FGS1R Long Term Stability Monitor for Position Mode* — A 6-orbit (total) test, distributed over cycle 7, monitors the Position Mode stability using a field in M35.

2. Proposal 7597, *FGS1R Long Term Stability Monitor for Transfer Mode* — This 7-orbit test obtains S-Curve data over the course of cycle 7 on standard star Upgren 69. It will establish a baseline of performance, and provide an indication of stability and thereby FGS1R's readiness to be used as a science instrument.

3. Proposal 7684, *HST Astrometry Angular Resolution Test* — is designed to compare the angular resolution of FGS1R and FGS3 in Transfer Mode (S-Curve data). A 9th magnitude known binary (component separation of 0.352 arcsec and relative magnitude of 0.6) will be observed at several (small) angular increments with both instruments. This test will not be performed until FGS1R stability is established and its S-Curves are re-optimized.

4. Proposal 7680, *FGS3 and FGS1R Transfer Mode Plate Scale Calibration* — used to check for any systematic effects, caused by misalignment of certain optical components, which may introduce spurious results in binary orbit programs.

7. Comparison of FGS3 and FGS1R

In order to illustrate the perfomance capabilities of FGS3 and FGS1R, we have generated a series of synthetic S-Curves of binary systems. A simple schematic of a binary orbit and resulting S-Curves are given in Figure 4. *The composite S-Curve of a multiple system is a linear superposition of the S-Curves from the individual components, scaled by their relative brightnesses.* If the components are widely separated, unique S-Curves are clearly in evidence as illustrated by the Y-axis S-Curve in Figure 4. Smaller separations yield a merged S-Curve with a morphology that differs from that of a single star (depending on the resolution of the instrument and the binary separation) as shown by the X-Axis S-Curve. The delineation of multiple components in the composite transfer function is accomplished by modelling the composite using a linear superposition of reference S-Curves from a single star, scaled by relative magnitude and shifted by the separation of the components.

The single star S-Curves of the current astrometer, FGS3, are shown in the upper two panels of Figure 5. These data were obtained at the center of the FGS, using the F583W filter on the standard star Upgren69. Clearly, the FGS3 Y-axis (left upper panel) exhibitis a near-perfect S-Curve in morphology and modulation, but the X-axis S-Curve is somewhat degraded in both amplitude and shape. If one compares these two panels with the solid-line S-Curves of FGS1R in Figure 2, it is evident that the FGS1R X *and* Y axes are nearly perfect and are comparable to the Y-axis of FGS3. The FGS3 X axis performance is what limits the FGS3's resolution and sensitivity and ultimately its ability to resolve binary systems with small separation and large brightness differences. Panels B and C in Figure 5 are composite S-Curves of binary systems that were synthetically generated from the FGS3 X and Y S-Curves: panel B is a 50 mas binary with a relative magnitude difference of 0 and panel C is a 50 mas binary with a delta magnitude of 2. From these figures it is clear the FGS3 can more easily resolve a binary along its Y-axis than along its X-axis. In panel c, for example, the morphology of the X-axis S-Curve more closely resembles that of a single star than do the Y-axis transfer functions. Please note however, the binary parameters used in these plots were chosen for visual graphical demonstration. In reality our data analysis tools would have no trouble resolving the binary in panel C's X-axis.

In anticipation of the enhanced performance of FGS1R, a study to assess and predict its expected performance was carried out at Lowell Observatory (Franz & Wasserman 1996). Since the Y-axis performance of FGS3 is near ideal it is a good representation of what can be expected from both axis of FGS1R. As stated earlier, the X-axis of FGS3 suffers from internal misalignments and therefore this axis is the limiting factor of FGS3's performance. The simulation study compared the X-axis performance of FGS3 to the Y-axis, with the X-axis representing FGS3, the Y-axis FGS1R. In essence, actual FGS3 data were used to generate both a table of synthetic binary observations and to provide a calibration database by which to de-convolve the simulated binaries.

For the simulation, the Lowell group used the data from a TRANSfer mode observation of a standard single star which was scanned 18 times. In order to avoid any possible correlation of the photometric noise from the individual scans, the observation was divided

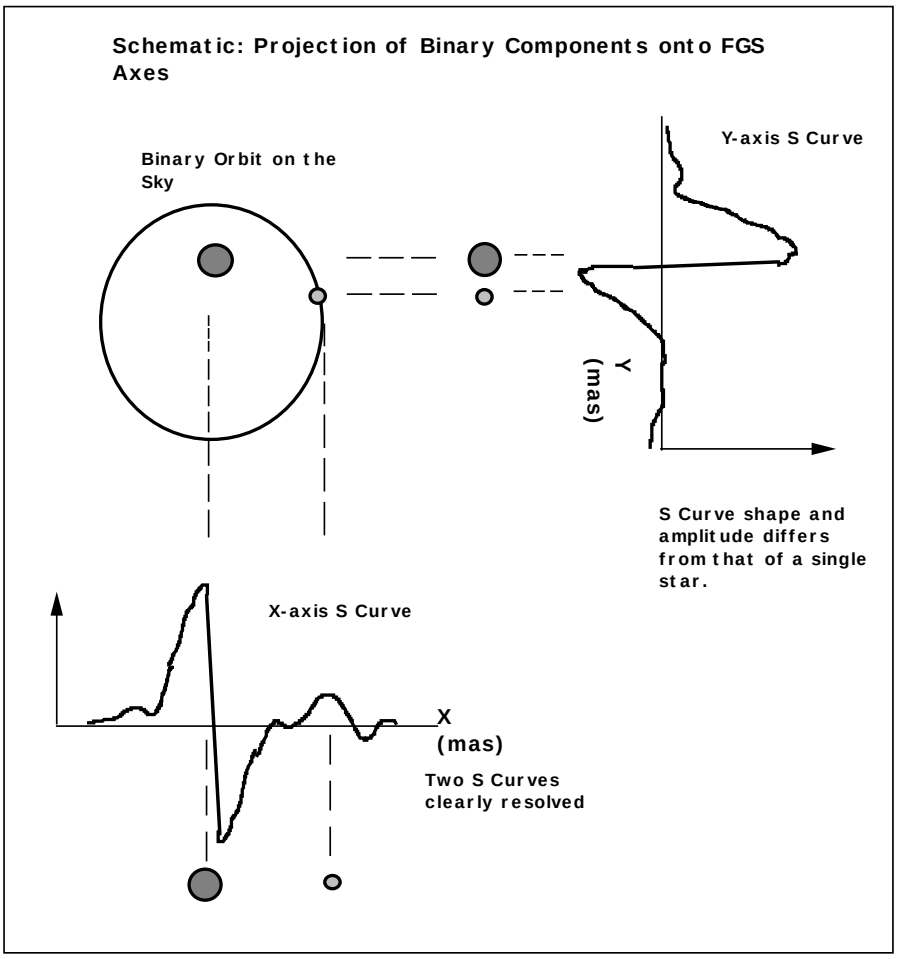

Figure 4. A schematic of a binary system projected onto the FGS X and Y axes. The separation of the components is large enough that the projection onto the FGS X-axis clearly shows two S-Curves. The Y-axis separation is much smaller and the composite S-Curve, although still noticeably different from a single S-Curve, will have to be modelled to deconvolve the components.

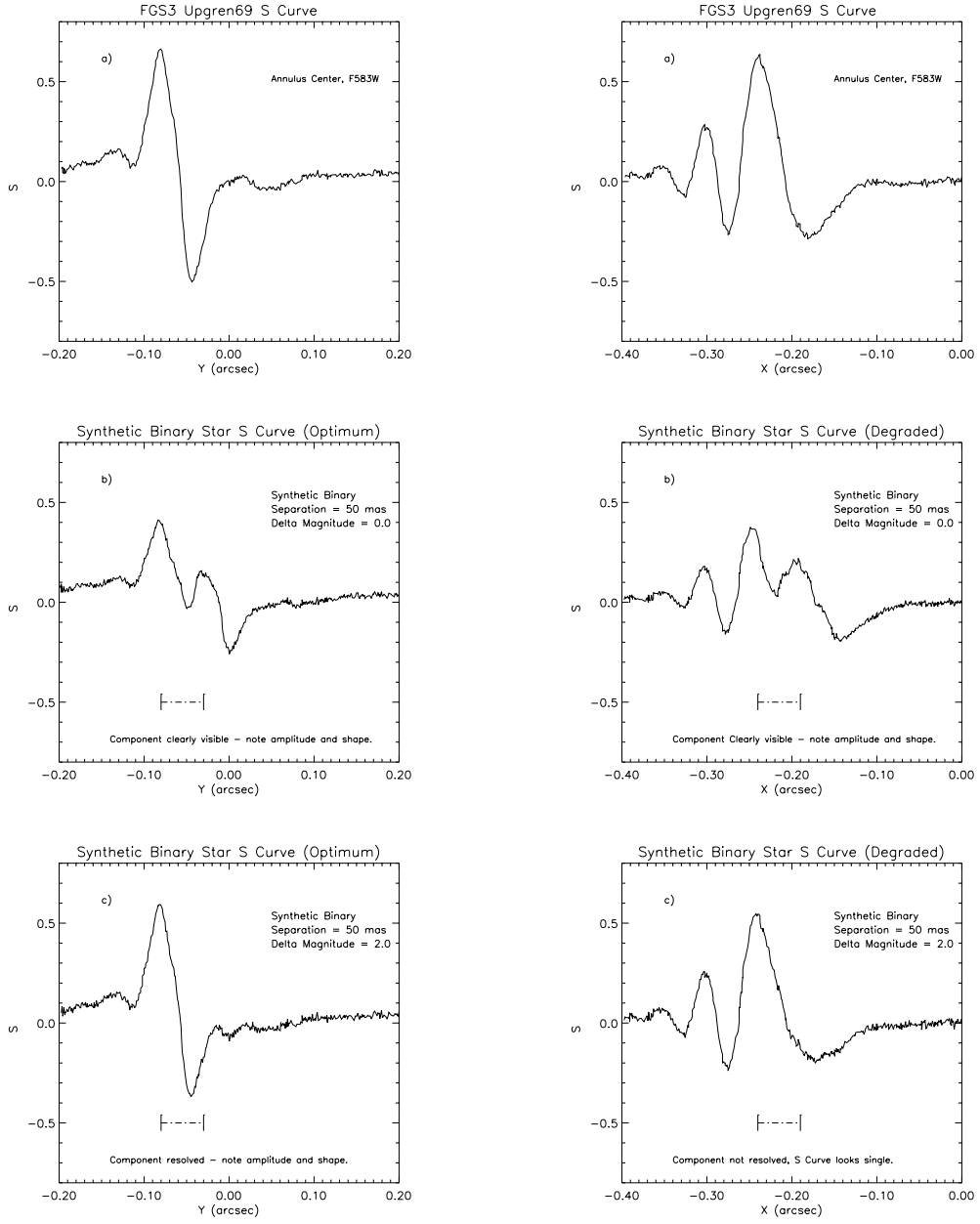

Figure 5. FGS3 S-Curves (panels "a") and synthetic composite S-Curves of binaries. The FGS3 Y-axis exhibits a near-perfect S-Curve and is representative of the S-Curves on both axes of FGS1R.

into 3 segments, one for each of the binary's two "components", and one for the calibration star. X and Y axis S-Curves were generated for a grid of binary star parameters, namely separations of 5, 10, 20, 30, and 80 milli-seconds of arc (mas) and with magnitude differences (δM) of 0.44, 1.51, 2.39, and 3.20 at each of the separations.

The results indicated that along the X-axis in FGS 3 the binary systems were not resolvable for these magnitude differences when the angular separation was less than 20 mas, and also at 20 mas the δM = 3.20 was not resolved. Along the Y-axis however, the "binary" was resolved when the separation was 10 mas for all but the δM = 3.2, and encouragingly, the non-singularity of the binary was "detected" at separation = 5mas for δM = 0.44 and 1.51, although it is not clear that it was actually "resolved".

This study was limited by considerations of signal to noise since each synthetic "observation" contained only 6 individual scans. This is also true for the calibration observations. Actual TRANSFER mode observations usually have between 15 and 35 scans and therefore yield significantly better S/N.

In summary, since the FGS3 y-axis S-Curve is about as good as those expected in both axis of FGS1R, these results suggest that FGS1R will be able, if stable and properly calibrated, to resolve multiple component star systems with angular separations as small as 10 mas, and to detect non-singularity at even smaller separations.

8. Summary

Initial results from the testing of FGS1R during the observatory verification period and initial months of Cycle 7 indicate that its performance exceeds that of FGS3 for astrometry science, that the articulating mirror adjustment works as planned and is crucial for achieving the original FGS design goals for astrometric resolution and sensitivity. Cycle 7 monitoring programs will provide the data needed for assessing the ultimate capabilities of the instrument and, if supported by the data, FGS1R will be calibrated as the HST astrometer in cycle 8. We have provided a temporal history of FGS1R and compared its capabilities with that of FGS3. Simulations show that when properly calibrated (and stable), FGS1R should be able to to resolve multiple component star systems with angular separations as small as 10 mas, and to detect non-singularity at even smaller separations.

Acknowledgments. We wish to thank Otto Franz and Larry Wasserman (Lowell Observatory) for their kindness, expertise, and for contributing many models and targets used for this manuscript and in the cycle calibration plans. We thank Linda Abramowicz-Reed and Kevin Chisolm of HDOS for their expertise on FGS1R and data analyses. We also express gratitude to Ed Kimmer and Gary Welter (GSFC) and Sherie Holfeltz, John Hershey, Denise Taylor, and Vicki Balzano for their expertise and help during SMOV, and Harry Payne, Antonella Nota (STScI), Barbara McArthur and Fritz G. Benedict (Univ. of Texas), and the Space Telescope Astrometry Team.

References

Abramowicz-Reed, L. and Chisolm, K., 1997, private communication.

Franz, O., and Wasserman, F. 1996, Minutes from the Space Telescope Astrometry Team Meeting, April 1996.

McArthur, B., and Benedict, G.F., 1997, this volume.

Voit, M., 1997, *HST Data Handbook*, Version 3.0 (Baltimore: STScI).